Composite Structures 92 (2010) 216–222

Contents lists available at ScienceDirect

Composite Structures

journal homepage: www.elsevier.com/locate/compstruct

An analytical model to study the effective stiffness of the composites with periodically distributed sphere particles

Y.P. Jiang *, K. Tohgo, Y. Shimamura

Department of Mechanical Engineering, Shizuoka University, 3-5-1 Johoku, Hamamatsu 432, Japan

ARTICLE INFO

Article history:
Available online 14 July 2009

Keywords:
Mori–Tanaka (M–T)
Particle reinforced composites (PRC)
Micro-mechanics
Hashin–Shtrikman (H–S) bounds
Microstructure

ABSTRACT

In order to analytically study the overall elastic stiffness of the composite containing periodically dispersed sphere particles, a new micro-mechanics model is developed in this paper. Three kinds of typical particle packing arrangements in the form of simple cubic lattice, body-centered cubic lattice and face-centered cubic lattice are considered and compared. The special characteristics of regular distribution are fully considered by incorporating the necessary geometrical symmetry conditions into strain Green's function. It is found that particle arrangement obviously affects the macroscopic elastic response of such the kind of composite. Moreover, most of the predictions by the present model are in good agreement with the FEM computations. The effective Young's modulus of BCC composite the effective shear modulus of SC composite are not in the range of the Hashin–Shtrikman bounds. The present model is also useful to verify some other numerical results mainly obtained by the unit-cell model, for instance, damage variables, matrix plasticity, etc.

1. Introduction

It is well known that particle arrangement in the matrix evidently affects the local stress/strain field, and in turn influences the macro-mechanics behaviors of the whole composite. Ganguly and Poole [1] calculated and compared the reinforcement stress for different reinforcement arrangements by using an iterative algorithm based on the two-dimensional representative volume element. Numerical results showed that particle stress is sensitive to the angular orientation of the neighboring reinforcements. Sun et al. [2] analyzed the effect of particle arrangement on stress concentration by using finite element method (FEM), and found that the stress concentration surrounding a particle is largely affected by the orientation of the two particles to each other. As a fundamental evidence for the existing computer simulations, Barfuss et al. [3] used a photo-elastic analogue to directly observe the local micro-stress field around two particles. However, most of the conventional effective medium methods, such as the Mori–Tanaka (M–T) model [4], self-consistent (SC) method [5], generalized self-consistent (GSC) model [6], double inclusion (DI) model [7], Ponte Castaneda Willis (PCW) model [8] and effective self-consistent (ESC) method [9], are originally proposed for studying the composite containing randomly distributed particles. They cannot well account for the effect of particle arrangement. Therefore, FEM and boundary element method (BEM) are often adopted to study the local stress field of the composite with periodical microstructures, i.e., all the particles are assumed to be regularly dispersed in the matrix. Generally, single-cell [10–15], double-cell [11,12] and four-cell [13,14] are usually selected for considering different particle distribution, and they are equivalent to simple cubic lattice, body-centered cubic lattice and face-centered cubic lattice, respectively. FEM is a powerful tool to establish the direct correlation of microstructures with material properties, but a lot of effort and time need to be cost on the construction of a geometry model and the corresponding meshing. Fortunately, many effective properties of a heterogeneous material often rely on their average response of the microstructures and properties of constituents, one does not need to construct a fairly complicated FEM model, and some micro-mechanics theories maybe more efficient in analyzing such problems. In the previous work, the authors [16,17] proposed an analytical method to study the effect of the interphase on the effective stiffness of the composite with regularly located particles. Now, this method is further extended and applied to many more composites with periodical microstructures.

The main objective of this research is to study the effective elastic properties of the composite reinforced by periodically distributed particles. In order to analytically predict the overall stiffness, a new micro-mechanics model will be developed. Three typical particle arrangements will be analyzed and compared, and the correctness of the present model is verified by the comparison with FEM.

* Corresponding author. Tel.: +81 053 478 1027.
E-mail address: ypjiang@nuaa.edu.cn (Y.P. Jiang).

0263-8223/$ - see front matter © 2009 Elsevier Ltd. All rights reserved.
doi:10.1016/j.compstruct.2009.07.010

2. The effective elastic stiffness of PRC

2.1. General expression for the strain field $\boldsymbol{\varepsilon}(\mathbf{x})$

In this paper, the terms for the reinforcement and matrix are represented by symbols with the subscripts 'P' and '0', respectively, and the overall terms of the composite are denoted by symbols with a over-line and tensors and vectors are denoted by bold face letters. Consider an infinite heterogeneous material with elasticity tensors $\mathbf{C}(\mathbf{x})$ at the point $\mathbf{x}$, and where an eigenstrain $\boldsymbol{\varepsilon}^*(\mathbf{x})$ (e.g., residue stress) is also in existence. Stress $\boldsymbol{\sigma}^0$ is applied at infinity if the material is homogeneous with elasticity tensor $\mathbf{C}_0$, i.e., having no inclusions, the corresponding strain field is denoted by $\boldsymbol{\varepsilon}^0$.

The total strain $\varepsilon_{mn}(\mathbf{x})$ is expressed by [18],

$$\varepsilon_{mn}(\mathbf{x}) = \varepsilon^0_{mn} + \int_V g_{mnij}(\mathbf{x}-\mathbf{x}') \cdot [C^0_{ijkl}(\mathbf{x}') \cdot \varepsilon^*_{kl}(\mathbf{x}') - \delta C_{ijkl}(\mathbf{x}') \cdot \varepsilon_{kl}(\mathbf{x}')] d\mathbf{x}' \tag{1}$$

with

$$\mathbf{C}(\mathbf{x}) = \mathbf{C}_0 + \delta\mathbf{C}(\mathbf{x}) \tag{2}$$

$$g_{mnij}(\mathbf{x}-\mathbf{x}') = -\frac{1}{2}[G_{mi,nj}(\mathbf{x}-\mathbf{x}') + G_{ni,mj}(\mathbf{x}-\mathbf{x}')] \tag{3}$$

where displacement Green's function $G_{kn}(\mathbf{x}-\mathbf{x}')$ in the infinite medium $\mathbf{C}_0$ gives the displacement in the direction k at point $\mathbf{x}$ when a unit force $f_i = \delta_{in}\delta(\mathbf{x}-\mathbf{x}')$ is applied at point $\mathbf{x}'$ in the direction n. δ_{in} is the Kronecker delta and $\delta(\mathbf{x}-\mathbf{x}')$ is the three-dimensional Dirac delta function, and $\mathbf{g}(\mathbf{x}-\mathbf{x}')$ is strain Green's function.

If the eigenstrain $\boldsymbol{\varepsilon}^*(\mathbf{x})$ is assumed to be zero, i.e., the inhomogeneity does not bear its own eigenstrain. Therefore, the following simple equation is reached.

$$\boldsymbol{\varepsilon}(\mathbf{x}) = \boldsymbol{\varepsilon}^0 - \int_V \mathbf{g}(\mathbf{x}-\mathbf{x}') \cdot [\mathbf{C}(\mathbf{x}') - \mathbf{C}_0] \cdot \boldsymbol{\varepsilon}(\mathbf{x}') d\mathbf{x}' \tag{4}$$

2.2. The equivalent elastic stiffness of PRC

Fig. 1 shows a schematic diagram for two sphere particles in the matrix, and the volume fraction of particles is denoted by f_P. Based on Eq. (4), the average strain in the particle is expressed by

$$\bar{\boldsymbol{\varepsilon}}_{\Omega_0} = \boldsymbol{\varepsilon}^0 - \mathbf{S} \cdot \mathbf{K}_P^{-1} \cdot \bar{\boldsymbol{\varepsilon}}_{\Omega_0} - \sum_{j=1}^{N} \frac{1}{\Omega_0} \int_{\Omega_0} \int_{\Omega_j} \mathbf{g}(\mathbf{x}-\mathbf{x}') \cdot \mathbf{K}_P^{-1} \cdot \bar{\boldsymbol{\varepsilon}}_{\Omega_j} d\mathbf{x}' d\mathbf{x} \tag{5}$$

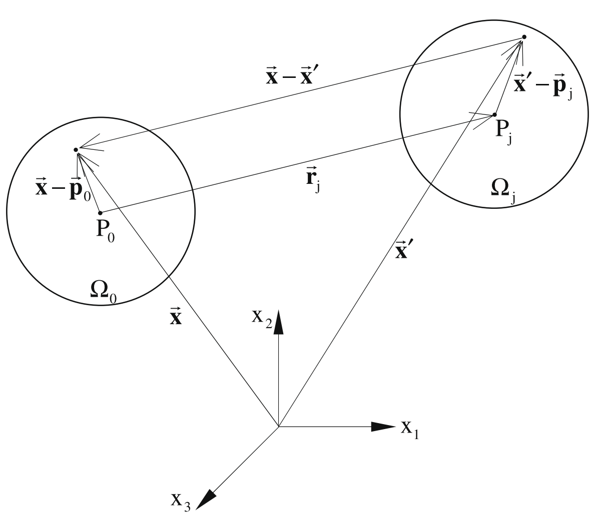

Fig. 1. Schematic diagram for two particles in a composite system.

where Ω_0 also represents the volume of the region Ω_0. Since $\bar{\varepsilon}_{\Omega_0} = \bar{\varepsilon}_{\Omega_j}$, the average strain in the region Ω_0 is expressed by

$$\bar{\boldsymbol{\varepsilon}}_{\Omega_0} = \mathbf{T} \cdot \boldsymbol{\varepsilon}^0 \tag{6}$$

with

$$\mathbf{T} = \left[\mathbf{I} + \mathbf{S} \cdot \mathbf{K}_P^{-1} + \sum_{j=1}^{N} \frac{1}{\Omega_0} \int_{\Omega_0} \int_{\Omega_j} \mathbf{g}(\mathbf{x}-\mathbf{x}') d\mathbf{x}' d\mathbf{x} \cdot \mathbf{K}_P^{-1}\right]^{-1} \tag{7}$$

here $\mathbf{I}$ denotes the four-ordered unit identity tensor. $\mathbf{S}$ is Eshelby's tensor for the sphere particle and listed in Appendix A, $\mathbf{K}_P$ are two fourth-order mismatch tensors, which are defined by $\mathbf{K}_P = (\mathbf{C}_P - \mathbf{C}_0)^{-1} \cdot \mathbf{C}_0$. So, the effective stiffness of PRC is expressed by

$$\overline{\mathbf{C}} = \mathbf{C}_0 \cdot [\mathbf{I} + f_P \mathbf{K}_P^{-1} \cdot \mathbf{T} \cdot \mathbf{A}^{-1}] \tag{8}$$

$$\mathbf{A} = \mathbf{I} - f_P \mathbf{S} \cdot \mathbf{K}_P^{-1} \cdot \mathbf{T} \tag{9}$$

3. Randomly and regularly distributed particles composite

3.1. Randomly distributed composites

The effective stiffness of composites $\overline{\mathbf{C}}$ is expressed by

$$\overline{\mathbf{C}} = \mathbf{C}_0 \cdot [\mathbf{I} + \mathbf{B} \cdot (\mathbf{I} - \mathbf{S} \cdot \mathbf{B})^{-1}] \tag{10}$$

with $\mathbf{B} = f_P(\mathbf{S} + \mathbf{K}_P)^{-1}$. It is worth noting that $\overline{\mathbf{C}}$ is a transversely isotropic tensor for the effective stiffness of PRC containing randomly located, aligned ellipsoid particles.

3.2. Regularly distributed composites

For the sake of simplicity, $\boldsymbol{\Pi} = \frac{1}{\Omega_0} \int_{\Omega_0} \int_{\Omega_j} \mathbf{g}(\mathbf{x}-\mathbf{x}') d\mathbf{x}' d\mathbf{x}$ is introduced. According to Jiang's conclusions in Ref. [16], $\boldsymbol{\Pi}$ is written as

$$\begin{aligned}\Pi = {} & \frac{\Omega_j}{40\pi(1-\nu_0)r^3}\Big[-75\frac{r_m r_n r_i r_j}{r^4} + 15\nu_0\Big(\frac{r_m r_i}{r^2}\delta_{jn} + \frac{r_n r_i}{r^2}\delta_{jm} + \frac{r_m r_j}{r^2}\delta_{in} \\ & + \frac{r_n r_j}{r^2}\delta_{im}\Big) + 15\frac{r_i r_j}{r^2}\delta_{mn} + 15(1-2\nu_0)\frac{r_m r_n}{r^2}\delta_{ij} - 5(1-2\nu_0)\delta_{ij}\delta_{mn} \\ & + 5(1-2\nu_0)(\delta_{im}\delta_{jn} + \delta_{in}\delta_{jm})\Big] + \frac{3\Omega_j a^2}{20\pi(1-\nu_0)r^5}\Big[35\frac{r_m r_n r_i r_j}{r^4} \\ & - 5\Big(\frac{r_m r_i}{r^2}\delta_{jn} + \frac{r_n r_i}{r^2}\delta_{jm} + \frac{r_m r_j}{r^2}\delta_{in} + \frac{r_n r_j}{r^2}\delta_{im}\Big) - 5\frac{r_i r_j}{r^2}\delta_{mn} \\ & - 5\frac{r_m r_n}{r^2}\delta_{ij} + \delta_{ij}\delta_{mn} + (\delta_{im}\delta_{jn} + \delta_{in}\delta_{jm})\Big]\end{aligned} \tag{11}$$

where $r = |\mathbf{x}-\mathbf{x}'|$, and a is the radius of sphere particle Ω_j.

Fig. 2 demonstrates PRCs with three typical particle packing arrangement, which are simple cubic (SC), body centered cubic (BCC) and face centered cubic (FCC). According to the geometrical symmetry conditions of particle packing arrangement, the above tensor $\boldsymbol{\Pi}$ can be further rephrased as,

$$\begin{aligned}\Pi_{\alpha\beta} = {} & \frac{\Omega_j}{8\pi(1-\nu_0)r^7}\begin{bmatrix} \Gamma_{11} & \Gamma_{12} & \Gamma_{13} & 0 & 0 & 0 \\ & \Gamma_{22} & \Gamma_{23} & 0 & 0 & 0 \\ & & \Gamma_{33} & 0 & 0 & 0 \\ & sym & & \Gamma_{44} & 0 & 0 \\ & & & & \Gamma_{55} & 0 \\ & & & & & \Gamma_{66} \end{bmatrix} \\ & - \frac{3\Omega_j a^2}{20\pi(1-\nu_0)r^9}\begin{bmatrix} T_{11} & T_{12} & T_{13} & 0 & 0 & 0 \\ & T_{22} & T_{23} & 0 & 0 & 0 \\ & & T_{33} & 0 & 0 & 0 \\ & sym & & T_{44} & 0 & 0 \\ & & & & T_{55} & 0 \\ & & & & & T_{66} \end{bmatrix}\end{aligned} \tag{12}$$

where $\alpha, \beta = 1–3$, the specific expressions of $\Gamma_{11}–\Gamma_{66}$ and $T_{11}–T_{66}$ are listed in Appendix A. After some algebra deductions, $\Pi_{\alpha\beta}$ is simplified as

$$\Pi_{\alpha\beta} = \left(\frac{\phi}{1-\upsilon_0}H_r^1 - \frac{2\phi^{5/3}}{1-\upsilon_0}H_r^2\right)M, \quad (r = \mathrm{SC, BCC, FCC}) \tag{13}$$

with

$$\phi = \frac{3f_P}{4\pi}, \quad M = \begin{bmatrix} -2 & 1 & 1 & 0 & 0 & 0 \\ & -2 & 1 & 0 & 0 & 0 \\ & & -2 & 0 & 0 & 0 \\ & sym & & 1 & 0 & 0 \\ & & & & 1 & 0 \\ & & & & & 1 \end{bmatrix}.$$

For the SC case, H_{SC}^1 and H_{SC}^2 are written as,

$$H_{SC}^1 = \lim_{n\to\infty}\sum_{k=-n}^{n}\sum_{j=-n}^{n}\sum_{i=-n}^{n}\frac{i^4+j^4+k^4-3i^2j^2-3i^2k^2-3j^2k^2}{6(i^2+j^2+k^2)^{7/2}} \approx 0.673 \tag{14.a}$$

$$H_{SC}^2 = \lim_{n\to\infty}\sum_{k=-n}^{n}\sum_{j=-n}^{n}\sum_{i=-n}^{n}\frac{7(i^4+j^4+k^4-3i^2j^2-3i^2k^2-3j^2k^2)}{30(i^2+j^2+k^2)^{9/2}} \approx 1.243 \tag{14.b}$$

For the BCC case, H_{BCC}^1 and H_{BCC}^2 are written as,

$$H_{BCC}^1 = \lim_{n\to\infty}\sum_{k=-n}^{n}\sum_{j=-n}^{n}\sum_{i=-n}^{n}\left\{\frac{(i+1/2)^4+(j+1/2)^4+(k+1/2)^4}{6[(i+1/2)^2+(j+1/2)^2+(k+1/2)^2]^{7/2}} - \frac{3(i+1/2)^2(j+1/2)^2+3(i+1/2)^2(k+1/2)^2+3(j+1/2)^2(k+1/2)^2}{6[(i+1/2)^2+(j+1/2)^2+(k+1/2)^2]^{7/2}}\right\} \approx -1.192 \tag{15.a}$$

$$H_{BCC}^2 = \lim_{n\to\infty}\sum_{k=-n}^{n}\sum_{j=-n}^{n}\sum_{i=-n}^{n}7\left\{\frac{(i+1/2)^4+(j+1/2)^4+(k+1/2)^4}{30[(i+1/2)^2+(j+1/2)^2+(k+1/2)^2]^{9/2}} - \frac{3(i+1/2)^2(j+1/2)^2+3(i+1/2)^2(k+1/2)^2+3(j+1/2)^2(k+1/2)^2}{30[(i+1/2)^2+(j+1/2)^2+(k+1/2)^2]^{9/2}}\right\} \approx -2.167 \tag{15.b}$$

For the FCC case, H_{FCC}^1 and H_{FCC}^2 are,

$$H_{FCC}^1 = \lim_{n\to\infty}\sum_{k=-n}^{n}\sum_{j=-n}^{n}\sum_{i=-n}^{n}\left\{\frac{(i+1/2)^4+j^4+(k+1/2)^4}{6[(i+1/2)^2+j^2+(k+1/2)^2]^{7/2}} - \frac{3(i+1/2)^2j^2+3(i+1/2)^2(k+1/2)^2+3j^2(k+1/2)^2}{6[(i+1/2)^2+j^2+(k+1/2)^2]^{7/2}}\right\} \approx -0.5316 \tag{16.a}$$

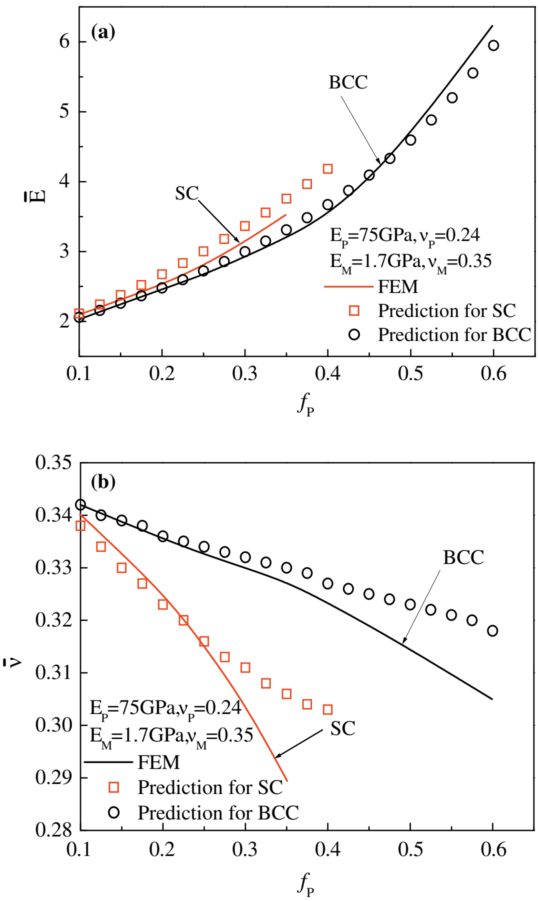

Fig. 3. Comparisons of Young's modulus (a) and Poisson's ratio (b) of the SC and BCC composites between FE results [11] and the present model.

$$H_{FCC}^2 = \lim_{n\to\infty}\sum_{k=-n}^{n}\sum_{j=-n}^{n}\sum_{i=-n}^{n}7\left\{\frac{(i+1/2)^4+j^4+(k+1/2)^4}{30[(i+1/2)^2+j^2+(k+1/2)^2]^{9/2}} - \frac{3(i+1/2)^2j^2+3(i+1/2)^2(k+1/2)^2+3j^2(k+1/2)^2}{30[(i+1/2)^2+j^2+(k+1/2)^2]^{9/2}}\right\} \approx -1.088 \tag{16.b}$$

For the SC composites, the tensor $\mathbf{T}_{SC}$ is,

$$\mathbf{T}_{SC} = \left[\mathbf{I} + \mathbf{S}\cdot\mathbf{K}_P^{-1} + \frac{0.673\phi - 2.486\phi^{5/3}}{1-\upsilon_0}M\cdot\mathbf{K}_P^{-1}\right]^{-1} \tag{17}$$

For the BCC composites, the tensor $\mathbf{T}_{BCC}$ is,

$$\mathbf{T}_{BCC} = \left[\mathbf{I} + \mathbf{S}\cdot\mathbf{K}_P^{-1} + \frac{-0.26\phi + 1.848(\phi/2)^{5/3}}{1-\upsilon_0}M\cdot\mathbf{K}_P^{-1}\right]^{-1} \tag{18}$$

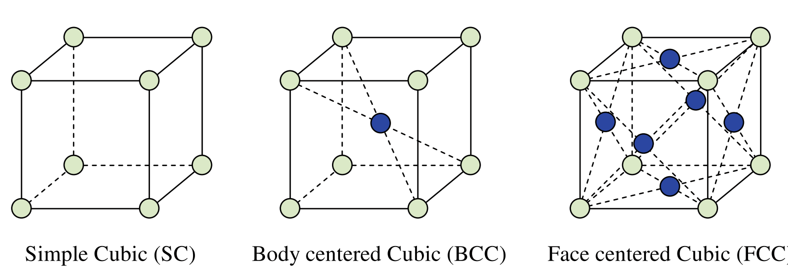

Fig. 2. Three typical particle packing arrangement for PRC.

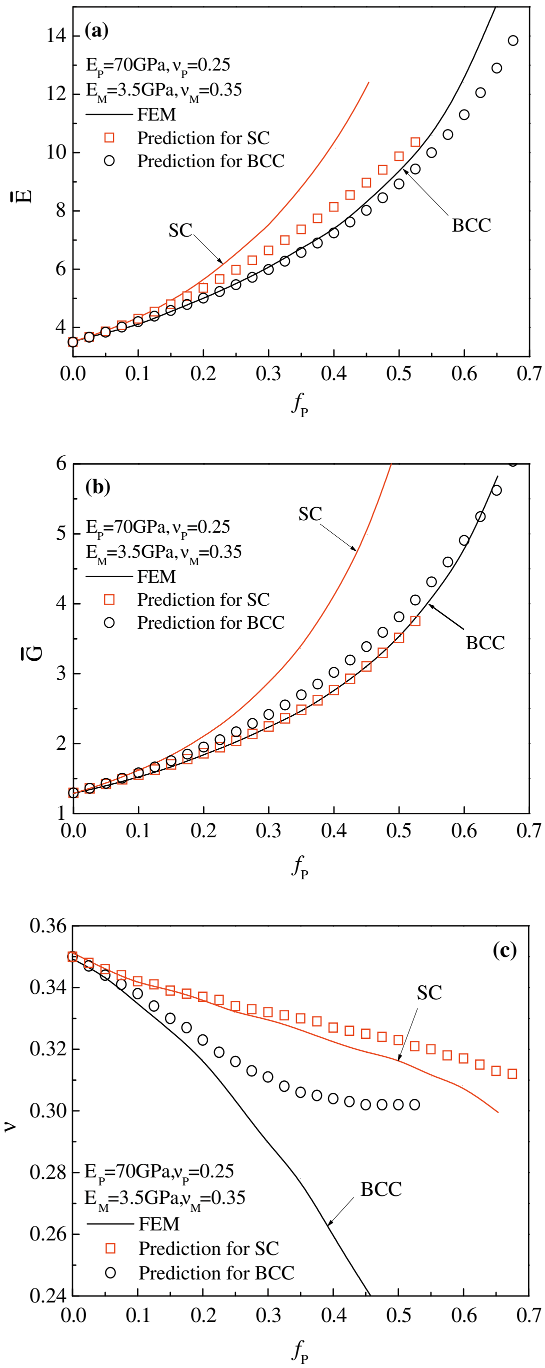

Fig. 4. Comparisons of Young's modulus (a), shear modulus (b) and Poisson's ratio (c) of the SC and BCC composites between FE results [12] and the present model.

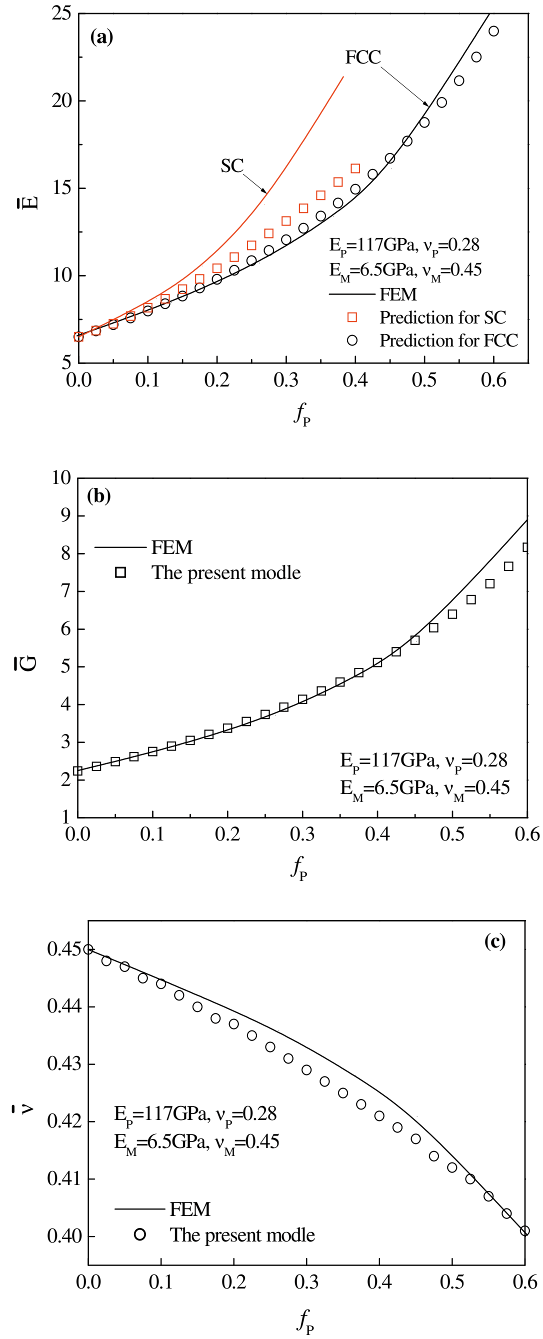

Fig. 5. Comparisons of Young's modulus (a) and shear modulus (b) and Poisson's ratio (c) of the SC and FCC composites between FE results [13] and the present model.

For the FCC composites, the tensor $\mathbf{T}_{FCC}$ is,

$$\mathbf{T}_{FCC} = \left[\mathbf{I} + \mathbf{S}\cdot\mathbf{K}_p^{-1} + \frac{0.0354\phi - 0.31(\phi/4)^{5/3}}{1-\upsilon_0} M\cdot\mathbf{K}_p^{-1}\right]^{-1} \tag{19}$$

The H–S bound is used to compare with the present model, and listed here,

$$\mathbf{C}_{HS} = \left\{\sum_r f_r\mathbf{C}_r\cdot[\mathbf{I}+\mathbf{S}\cdot\mathbf{C}_*^{-1}\cdot(\mathbf{C}_r-\mathbf{C}_*)]^{-1}\right\} \times \left\{\sum_r f_r[\mathbf{I}+\mathbf{S}\cdot\mathbf{C}_*^{-1}\cdot(\mathbf{C}_r-\mathbf{C}_*)]^{-1}\right\}^{-1} \tag{20}$$

The H–S upper and lower bounds are separately determined by choosing $\mathbf{C}_*$ as the largest and lowest stiffness among the constituents.

4. Results and discussion

Firstly, the exactness of the present model should be verified, and five cases of FEM results are used for the comparison with the present predictions. Predictions with the classic M–T method are also listed for every case at the same time. Fig. 3a and b shows the predictions of the overall Young's and Poisson's ratio of PRC with the SC and BCC distributions, respectively. The comparisons with the FEM results [11] show that the present model can predicts

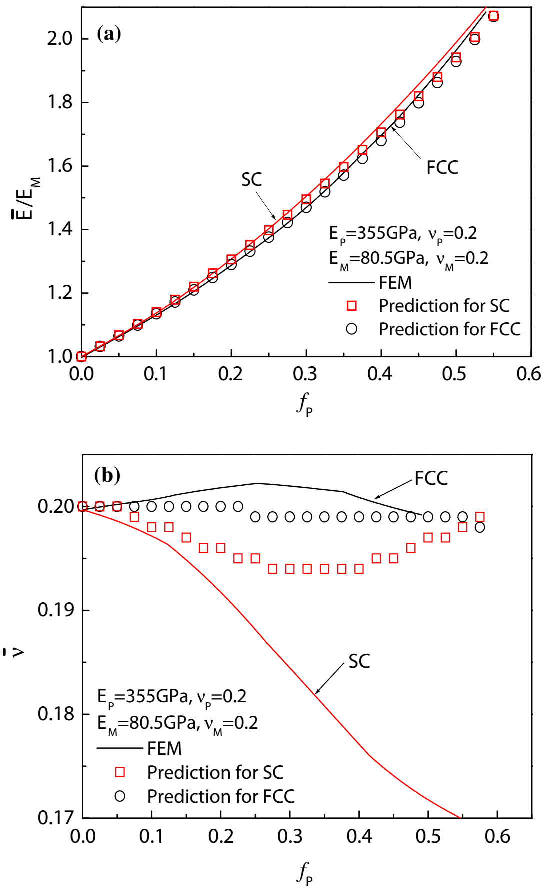

Fig. 6. Comparisons of Young's modulus (a) and Poisson's ratio (b) of the SC and FCC composites between FE results [14] and the present model.

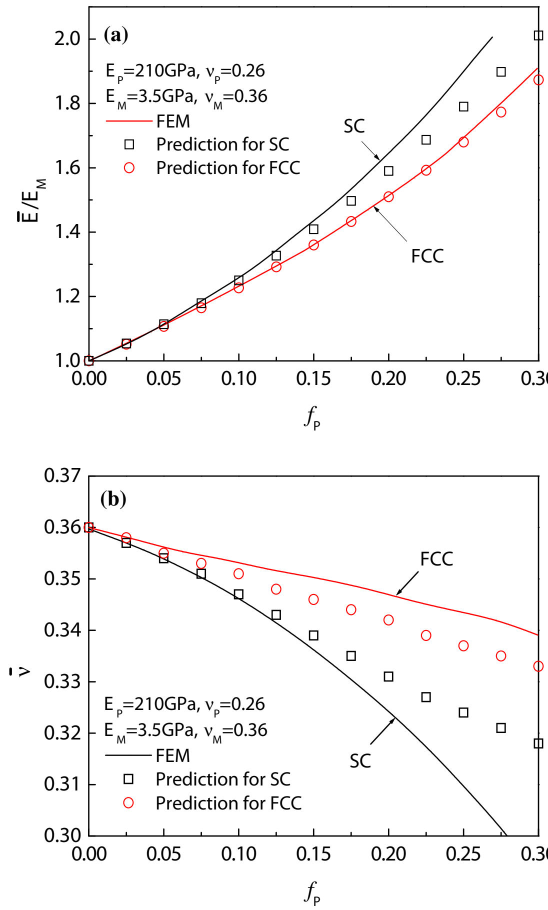

Fig. 7. Comparisons of Young's modulus (a) and Poisson's ratio (b) of the SC and FCC composites between FE results [14] and the present model.

the overall stiffness of the composites very well. Material properties are: $E_P = 75$ GPa, $\nu_P = 0.24$, $E_M = 1.7$ GPa, $\nu_M = 0.35$. Figs. 4–7 show the comparisons of (a) Young's modulus and (b) Poisson's ratio of the composites between FE results and the present model for different material systems. In Fig. 4, material properties are [12]: $E_P = 70$ GPa, $\nu_P = 0.25$, $E_M = 3.5$ GPa, $\nu_M = 0.35$. In Fig. 5, material properties are [13]: $E_P = 117$ GPa, $\nu_P = 0.28, E_M = 6.5$ GPa, $\nu_M = 0.45$. In Fig. 6, material properties are [14]: $E_P = 355$ GPa, $\nu_P = 0.2$, $E_M = 80.5$ GPa, $\nu_M = 0.2$. In Fig. 7, material properties are [14]: $E_P = 210$ GPa, $\nu_P = 0.26$, $E_M = 3.5$ GPa, $\nu_M = 0.36$. Most of the predictions are in good agreement with the corresponding FE results. Compare to the predictions of the BCC case and FCC case, the predictions of the SC composite deviate from the corresponding FEM results.

Comparisons show that the discrepancy between the predicted Poisson ratios by FEM and the present method are very high, and which would be explained as follows. In the FEM computation, since the strain fields in the particle and matrix are different, and thus the applied surface and side surfaces of the unit-cell model would not be plane after the deformation. This problem is not very serious for the prediction of the tensile and shear modulus, which can be easily solved by applying the displacement boundary and summing the reaction force over all the elements located in the applied surface. But it is not easy to predict the effective Poisson's ratio by the same method. For the sake of simplicity and convenience, some compulsory boundary conditions, such as multi-points constraint, should be enforced on the applied and lateral planes. However, there is no such extra restraint in the real composite materials, and such kind of treatment inevitably brings about a large errors. As expected, the error would increase with increasing the volume fraction of particles for the SC and BCC cases, and which is obviously displayed in Figs. 3b, 4c, 6b and 7b. For the FCC case, since the particle density on every surface is relatively uniform, so the induced error by the special boundary conditions is lower than the other cases.

Fig. 8 shows the comparison of the overall Young's modulus (a), Shear modulus (b) and Poisson's ratio (c) of the composite with different particle arrangements predicted by the present model, M–T method and H–S bounds [19]. Material properties used here are as follows: $E_P = 70$ GPa, $\nu_P = 0.25$, $E_M = 1.7$ GPa, $\nu_M = 0.35$. Particle arrangement affects the macro-mechanics behavior of the composites. After comparing these results, at the same volume fraction of particles, the sequence for the Young's modulus of different arrangement is, SC > FCC > M–T > BCC, and the sequence for the shear modulus is, SC < FCC < M–T < BCC. Additionally, the difference between the FCC case and the M–T predictions for all the effective moduli and Poisson's ratio is very small, even can be neglected to some extent. The effective Young's modulus of BCC composite the effective shear modulus of SC composite exceed the range of the H–S bounds, and the predictions by the classical M–T method coincides with the H–S lower bound.

5. Conclusions

A new micro-mechanics model is proposed for studying the effective elastic modulus of the composites containing regularly distributed sphere particles. Three typical particle arrangements in the form of simple cubic lattice, body-centered cubic lattice and face-centered cubic lattice are investigated. Most of the predic-

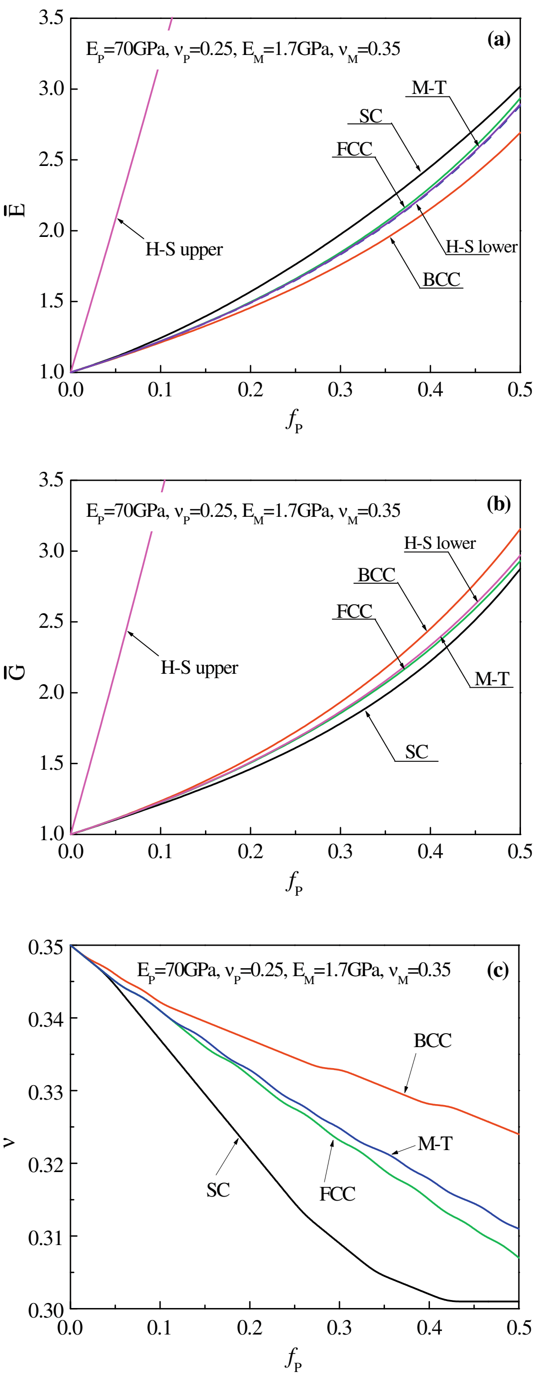

Fig. 8. Comparison of the overall Young's modulus (a), shear modulus (b) and Poisson's ratio (c) of the composites with different particle arrangements between the present model, M–T method and H–S bounds [19].

tions by the present model are in good agreement with FEM results. Several important conclusions are reached.

[1] Particle distribution has an obvious effect on the macro-mechanics behavior of the composites. As for the Young's modulus of the composites with the same volume fraction of particles, the sequence of different arrangement is, SC > FCC > M–T > BCC, and as for the shear modulus, the sequence is, SC < FCC < M–T < BCC.

[2] The effective elastic properties of the FCC composite are very near to the predictions of the M–T method, i.e., the overall elastic properties of the FCC composite are very equivalent to those of the random composite.

[3] The effective Young's modulus of the BCC composite the effective shear modulus of the SC composite are not in the range of the H–S bounds, and predictions with the M–T method coincide with the H–S lower bound.

Acknowledgement

This research was supported by a Grant-in-Aid for JSPS Fellows (20.08058) from the Ministry of Education, Science, Sports and Culture of Japan.

Appendix A

$$\begin{aligned}
\Gamma_{11} &= (-8+4v_0)r_1^4 + (1-2v_0)r_2^4 + (1-2v_0)r_3^4 + (8+2v_0)r_1^2r_2^2 \\
&\quad + (8+2v_0)r_1^2r_3^2 + (2-4v_0)r_2^2r_3^2 \\
\Gamma_{22} &= (1-2v_0)r_1^4 + (-8+4v_0)r_2^4 + (1-2v_0)r_3^4 + (8+2v_0)r_1^2r_2^2 \\
&\quad + (2-4v_0)r_1^2r_3^2 + (8+2v_0)r_2^2r_3^2 \\
\Gamma_{33} &= (1-2v_0)r_1^4 + (1-2v_0)r_2^4 + (-8+4v_0)r_3^4 + (2-4v_0)r_1^2r_2^2 \\
&\quad + (8+2v_0)r_1^2r_3^2 + (8+2v_0)r_2^2r_3^2 \\
\Gamma_{12} &= (2-4v_0)r_1^4 + (2+2v_0)r_2^4 - (1-2v_0)r_3^4 - (11+2v_0)r_1^2r_2^2 \\
&\quad + (1-2v_0)r_1^2r_3^2 + (1+4v_0)r_2^2r_3^2 \\
\Gamma_{13} &= (2-4v_0)r_1^4 - (1-2v_0)r_2^4 + (2+2v_0)r_3^4 + (1-2v_0)r_1^2r_2^2 \\
&\quad - (11+2v_0)r_1^2r_3^2 + (1+4v_0)r_2^2r_3^2 \\
\Gamma_{23} &= -(1-2v_0)r_1^4 + (2-4v_0)r_2^4 + (2+2v_0)r_3^4 + (1-2v_0)r_1^2r_2^2 \\
&\quad + (1+4v_0)r_1^2r_3^2 - (11+2v_0)r_2^2r_3^2 \\
\Gamma_{44} &= (1-2v_0)r_1^4 + (1+v_0)r_2^4 + (1+v_0)r_3^4 - (13-2v_0)r_2^2r_3^2 \\
&\quad + (2-v_0)r_1^2r_3^2 + (2-v_0)r_1^2r_2^2 \\
\Gamma_{55} &= (1+v_0)r_1^4 + (1-2v_0)r_2^4 + (1+v_0)r_3^4 + (2-v_0)r_2^2r_3^2 \\
&\quad - (13-2v_0)r_1^2r_3^2 + (2-v_0)r_1^2r_2^2 \\
\Gamma_{66} &= (1+v_0)r_1^4 + (1+v_0)r_2^4 + (1-2v_0)r_3^4 + (2-v_0)r_2^2r_3^2 \\
&\quad + (2-v_0)r_1^2r_3^2 - (13-2v_0)r_1^2r_2^2 \\
T_{11} &= 8r_1^4 + 3r_2^4 + 3r_3^4 + 6r_2^2r_3^2 - 24r_1^2r_3^2 - 24r_1^2r_2^2 \\
T_{22} &= 3r_1^4 + 8r_2^4 + 3r_3^4 - 24r_2^2r_3^2 + 6r_1^2r_3^2 - 24r_1^2r_2^2 \\
T_{33} &= 3r_1^4 + 3r_2^4 + 8r_3^4 - 24r_2^2r_3^2 - 24r_1^2r_3^2 + 6r_1^2r_2^2 \\
T_{12} &= -4r_1^4 - 4r_2^4 + r_3^4 + 27r_1^2r_2^2 - 3r_1^2r_3^2 - 3r_2^2r_3^2 \\
T_{13} &= -4r_1^4 + r_2^4 - 4r_3^4 - 3r_1^2r_2^2 + 27r_1^2r_3^2 - 3r_2^2r_3^2 \\
T_{23} &= r_1^4 - 4r_2^4 - 4r_3^4 - 3r_1^2r_2^2 - 3r_1^2r_3^2 + 27r_2^2r_3^2 \\
T_{44} &= r_1^4 - 4r_2^4 - 4r_3^4 - 3r_1^2r_2^2 - 3r_1^2r_3^2 + 27r_2^2r_3^2 \\
T_{55} &= -4r_1^4 + r_2^4 - 4r_3^4 - 3r_1^2r_2^2 + 27r_1^2r_3^2 - 3r_2^2r_3^2 \\
T_{66} &= -4r_1^4 - 4r_2^4 + r_3^4 + 27r_1^2r_2^2 - 3r_1^2r_3^2 - 3r_2^2r_3^2
\end{aligned}$$

where, r_1, r_2, r_3 are the three coordinates of the particle center.

References

[1] Ganguly P, Poole WJ. Influence of reinforcement arrangement on the local reinforcement stresses in composite materials. J Mech Phys Solids 2004;52(6):1355–77.
[2] Sun CJ, Saffari P, Sadeghipour K, Baran G. Effects of particle arrangement on stress concentrations in composites. Mater Sci Eng A 2005;405(1):287–95.
[3] Barfuss J, Dryden JR, Shinozaki DM. Use of photoelasticity to study the effect of particle distribution on stress in composites. Mater Sci Eng A 1995;202(1):57–62.
[4] Mori T, Tanaka K. Average stress in matrix and average elastic energy of materials with misfitting inclusions. Acta Metall Mater 1973;21(5):571–4.
[5] Hershey AV. The elasticity of an isotropic aggregate of anisotropic crystals. J Appl Mech 1954;21:226–40.

[6] Christensen RM, Lo KH. Solutions for effective shear properties in three phase sphere and cylinder models. J Mech Phys Solids 1979;27(4):315–30.
[7] Hori M, Nemat-Nasser S. Double-inclusion model and overall moduli of multi-phase composites. Mech Mater 1993;14(3):189–206.
[8] Castaneda PP, Willis JR. The effect of spatial distribution on the effective behavior of composite materials and cracked media. J Mech Phys Solids 1995;43(12):1919–51.
[9] Zheng QS, Du DX. An explicit and universally applicable estimate for the effective properties of multiphase composites which accounts for inclusion distribution. J Mech Phys Solids 2001;49(11):2765–88.
[10] Jiang YP, Guo WL, Yang H. Numerical studies on the effective shear modulus of particle reinforced composites with an inhomogeneous interphase. Comput Mater Sci 2008;43(4):724–31.
[11] Sun CJ, Saffari P, Ranade R, Sadeghipour K, Baran G. Finite element analysis of elastic property bounds of a composite with randomly distributed particles. Compos: A 2007;38:80–6.
[12] Muliana AH, Kim JS. A concurrent micromechanical model for predicting nonlinear viscoelastic responses of composites reinforced with solid spherical particles. Int J Solids Struct 2007;44(21):6891–913.
[13] Balac I, Milovancevic M, Tang C, Uskokovic PS, Uskokovic DP. Estimation of elastic properties of a particulate polymer composite using a face-centered cubic FE model. Mater Lett 2004;58(19):2437–41.
[14] Llorca J, Elices M, Termonia Y. Elastic properties of sphere-reinforced composites with a mesophase. Acta Mater 2000;48(18):4589–97.
[15] Tsui CP, Tang CY, Lee TC. Prediction for debonding damage process of glass beads-reinforced modified polyphenylene oxide under simple shear. J Mater Process Technol 2001;117(1):105–10.
[16] Jiang YP, Tohgo K, Shimamura Y. A micro-mechanics model for composites reinforced by particles with an inhomogeneous interphase. Comput Mater Sci 2009;46:507–15.
[17] Jiang YP, Guo WL, Yang H. Numerical studies on the effective shear modulus of particle reinforced composites with an inhomogeneous interphase. Comput Mater Sci 2008;43(4):724–31.
[18] Berveiller M, Fassi-Fehri O, Hihi A. The problem of tow plastic and heterogeneous inclusions in an anisotropic medium. Int J Eng Sci 1987;25(6):691–709.
[19] Hashin Z. On elastic behaviour of fibre reinforced materials of arbitrary transverse phase geometry. J Mech Phys Solids 1965;13(3):119–34.